Technical University of Denmark

DTU

Raman and loss induced quantum noise in depleted fiber optical parametric amplifiers

Friis, Søren Michael Mørk; Rottwitt, Karsten; McKinstrie, C. J.

DTU Library
Technical Information Center of Denmark

Raman and loss induced quantum noise in depleted fiber optical parametric amplifiers

S. M. M. Friis,[1,*] **K. Rottwitt,**[1] **and C. J. McKinstrie**[2]

[1]*Department of Photonics Engineering, Technical University of Denmark, 2800 Kongens Lyngby, Denmark*
[2]*Bell Laboratories, Alcatel Lucent, Holmdel, New Jersey, 07733, USA*

[*]*smmf@fotonik.dtu.dk*

Abstract: We present a semi-classical approach for predicting the quantum noise properties of fiber optical parametric amplifiers. The unavoidable contributors of noise, vacuum fluctuations, loss-induced noise, and spontaneous Raman scattering, are included in the analysis of both phase-insensitive and phase-sensitive amplifiers. We show that the model agrees with earlier fully quantum approaches in the linear gain regime, whereas in the saturated gain regime, in which the classical equations are valid, we predict that the amplifier increases the signal-to-noise ratio by generating an amplitude-squeezed state of light. Also, in the same process, we analyze the quantum noise properties of the pump, which is difficult using standard quantum approaches, and we discover that the pump displays complicated dynamics in both the linear and the nonlinear gain regimes.

© 2013 Optical Society of America

References and links

1. J. Hansryd, P. A. Andrekson, M. Westlund, J. Li, and P. Hedekvist, "Fiber-based optical parametric amplifiers and their applications," IEEE J. Sel. Top. Quantum Electron. **8**, 506–520 (2002).
2. J. A. Levenson, I. Abram, T. Rivera, and P. Grangier, "Reduction of quantum noise in optical parametric amplification," J. Opt. Soc. Am. B **10**, 2233–2238 (1993).
3. C. M. Caves, "Quantum limits on noise in linear amplifiers," Phys. Rev. D **26**, 1817–1839 (1982).
4. Z. Tong, C. Lundström, P. A. Andrekson, C. J. McKinstrie, M. Karlsson, D. J. Blessing, E. Tipsuwannakul, B. J. Puttnam, H. Toda, and L. Grüner-Nielsen, "Towards ultrasensitive optical links enabled by low-noise phase-sensitive amplifiers," Nat. Photonics **5**, 340–436 (2011).
5. C. J. McKinstrie and J. P. Gordon, "Field fluctuations produced by parametric processes in fibers," IEEE J. Sel. Top. Quantum Electron. **18**, 958–969 (2012).
6. C. J. McKinstrie and S. Radic, "Phase-sensitive amplification in a fiber," Opt. Express **12**, 4973–4979 (2004).
7. C. J. McKinstrie, J. D. Harvey, S. Radic, and M. G. Raymer, "Translation of quantum states by four-wave mixing in fibers," Opt. Express **13**, 9131–9142 (2005).
8. C. J. McKinstrie, M. Yu, M. G. Raymer, and S. Radic, "Quantum noise properties of parametric processes," Opt. Express **13**, 4986–5012 (2005).
9. C. J. McKinstrie, M. G. Raymer, S. Radic, and M. V. Vasilyev, "Quantum mechanics of phase-sensitive amplification in a fiber," Opt. Commun. **257**, 146–163 (2005).
10. P. L. Voss and P. Kumar, "Raman-effect induced noise limits on $\chi^{(3)}$ parametric amplifiers and wavelength converters," J. Opt. B Quantum Semiclassical Opt. **6**, 762–770 (2004).
11. P. L. Voss, K. G. Köprülü, and P. Kumar, "Raman-noise-induced quantum limits for $\chi^{(3)}$ nondegenerate phase-sensitive amplification and quadrature squeezing," J. Opt. Soc. Am. B **23**, 598–609 (2006).
12. G. P. Agrawal, *Nonlinear Fiber Optics* (Academic, 2007).

13. H. Kidorf, K. Rottwitt, M. Nissov, M. Ma, and E. Rabarijaona, "Pump interactions in a 100-nm bandwidth Raman amplifier," IEEE Photonics Technol. Lett. **11**, 530–532 (1999).
14. R. H. Stolen, J. P. Gordon, W. J. Tomlinson, and H. A. Haus, "Raman response function of silica-core fibers," J. Opt. Soc. Am. B **6**, 1159–1166 (1989).
15. K. Rottwitt, J. Bromage, A. J. Stentz, L. Leng, M. E. Lines, and H. Smith, "Scaling of the Raman gain coefficient: Applications to germanosilicate fibers," J. Lightwave Technol. **21**, 1652–1662 (2003).
16. A. S. Y. Hsieh, G. K. L. Wong, S. G. Murdoch, S. Coen, F. Vanholsbeeck, R. Leonhardt, and J. D. Harvey, "Combined effect of Raman and parametric gain on single-pump parametric amplifiers," Opt. Express **15**, 8104–8114 (2007).
17. C. J. McKinstrie and M. G. Raymer, "Four-wave-mixing cascades near the zero-dispersion frequency," Opt. Express **14**, 9600–9610 (2006).
18. Z. Tong, C. Lundström, P. A. Andrekson, M. Karlsson, and A. Bogris, "Ultralow noise, broadband phase-sensitive optical amplifiers, and their applications," IEEE J. Sel. Top. Quantum Electron. **18**, 1016–1032 (2012).
19. M. Vasilyev, "Distributed phase-sensitive amplification," Opt. Express **13**, 7563–7571 (2005).
20. C. C. Gerry and P. L. Knight, *Introductory Quantum Optics* (Cambridge University, 2005).
21. C. J. McKinstrie, S. Radic, R. M. Jopson, and A. R. Chraplyvy, "Quantum noise limits on optical monitoring with parametric devices," Opt. Commun. **259**, 309–320 (2006).
22. K. Rottwitt and A. J. Stentz, "Raman amplification in lightwave communication systems," in *Optical Fiber Telecommunications IV-A*, I. Kaminow and T. Li, eds. (Academic, 2002), pp. 213–257.
23. Z. Tong, A. Bogris, M. Karlsson, and P. A. Andrekson, "Full characterization of the signal and idler noise figure spectra in single-pumped fiber optical parametric amplifiers," Opt. Express **18**, 2884–2893 (2010).
24. K. Croussore and G. Li, "Phase and amplitude regeneration of differential phase-shift keyed signals using phase-sensitive amplification," IEEE J. Sel. Top. Quantum Electron. **14**, 648–658 (2008).
25. M. Sköld, J. Yang, H. Sunnerud, M. Karlsson, S. Oda, and P. A. Andrekson, "Constellation diagram analysis of DPSK signal regeneration in a saturated parametric amplifier," Opt. Express **16**, 5974–5982 (2008).
26. C. Peucheret, M. Lorenzen, J. Seoane, D. Noordegraaf, C. V. Nielsen, L. Grüner-Nielsen, and K. Rottwitt, "Amplitude regeneration of RZ-DPSK signals in single-pump fiber-optic parametric amplifiers," IEEE Photonics Technol. Lett. **21**, 872–874 (2009).
27. M. Matsumoto, "Fiber-based all-optical signal regeneration," IEEE J. Sel. Top. Quantum Electron. **18**, 738–752 (2012).

1. Introduction

Fiber optical parametric amplifiers (FOPAs) have many potential applications in future all-optical communication systems. Compared to today's commercialized EDFA and Raman amplifiers, the most distinct properties of FOPAs are: their ability to operate as phase-sensitive amplifiers (PSA); their inherent generation of a frequency shifted copy of the signal called the idler [1]; and low-noise amplification performance [2]. PSAs have been shown to break the 3-dB quantum-limited noise figure (NF) of traditional phase-insensitive amplifiers (PIA) by amplifying only in-phase noise fluctuations while attenuating others, thus achieving a theoretical minimum of 0-dB NF [3]. Today, the lowest NF measured is 1.1 dB [4], with a 26.5-dB parametric gain. The idler generated at the opposite side-band of the signal relative to the pump enables transparent wavelength conversion, phase conjugation and monitoring in all-fiber optical networks. Even though parametric amplification can be realized in both $\chi^{(2)}$- and $\chi^{(3)}$-based materials, we only focus on silica fibers in this work, from which $\chi^{(2)}$ effects are absent.

Parametric processes based on four-wave mixing (FWM) exist in a number of different frequency configurations [5]. In Fig. 1, six different configurations are shown: (a), modulational interaction, is the simplest approach used for parametric amplification or frequency conversion, in which two pump (p) photons annihilate and create one photon at both signal (s) and idler (i) frequencies. The amplifier operates phase-insensitively (PI) or phase-sensitively (PS) depending on whether the idler is absent or present at the input. Next in (b), inverse modulational interaction, one photon from each pump annihilates and creates two signal photons; the signal then interacts with itself rather than with the idler, thus making the process always phase-sensitive. The processes (c) and (d) are generalized configurations of (a) and (b), respectively (Fig. 1 thus contains an actual number of four configurations), where no wave components in the FWM process are degenerate. These two FWM processes are called phase-conjugation
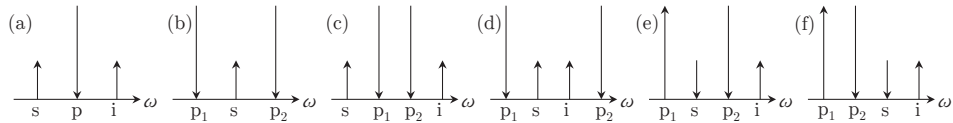
Fig. 1. Schematics of six different configurations of parametric processes based on four-wave mixing, {p, s, i} denote pump, signal and idler, respectively.

processes, because the generated idler is proportional to the complex conjugate of the amplified signal [6]. In the processes (a)-(d), the amplified waves grow exponentially. The last two processes, (e) and (f), are labeled distant and nearby Bragg scattering, from the possible applications of distant and nearby frequency conversion. They distinguish themselves from the former configurations by transferring power between the signal and idler (and between the two pumps) periodically through the fiber; the pumps do not amplify either of the signal or idler, but FWM enables the conversion of power. The generated idler is directly proportional to the signal, so no phase-conjugation takes place [7]. Also, the Bragg scattering processes do not suffer from the 3-dB NF, which is unavoidable in PI amplification, because the total sideband power is conserved and therefore no vacuum fluctuations are amplified. Depending on how the configurations (a)–(f) are chosen relative to the zero-dispersion-frequency (ZDF), the three processes of modulational interaction, phase conjugation and Bragg scattering may take place separately or simultaneously.

The quantum noise properties of the mentioned parametric processes are analyzed in [5, 8, 9] from a quantum mechanical point of view, in which the pumps are treated classically and as constants. Raman scattering is included in [10, 11], while still assuming a classical, constant pump. Consequently, the results of these works are only valid in the linear gain regime, in which the pump remains essentially undepleted by the signal and idler. Until the quantum equations of motion for the full system of four quantum waves are solved analytically, one must rely on semi-classical approaches to analyze quantum noise in the nonlinear gain regime.

In this paper, we present a semi-classical method for describing quantum noise in parametric processes, which is valid in the linear as well as in the nonlinear gain regimes. The method includes the effects of FWM, loss and Raman scattering, and their respective implications on the noise properties of parametric processes. We consider only case (a) of Fig. 1, but any of the configurations (a)–(f) could be analyzed by the semi-classical approach presented here. Furthermore, the quantum fluctuations of the pump are treated similarly to the fluctuations of the signal and idler, which allows us to investigate the noise properties of the pump both in the linear as well as in the nonlinear gain regimes. This is opposed to existing, approximate quantum approaches that always treat the pump classically to ease analytical calculations.

The paper is structured as follows: In Sec. 2 the classical equations describing FWM, loss and Raman scattering in a fiber are presented, and the classical approaches to simulate the coherent state of light and spontaneous emission are defined. In Sec. 3, both PI and PS parametric amplifiers are simulated in the linear gain regime and the impact of distributed loss and spontaneous Raman scattering on the signal-to-noise ratio (SNR) of an amplified signal is investigated. Section 4 presents the results of the classical model when an amplifier is configured to significantly deplete the pump, and Sec. 5 summarizes the paper.

2. Theory and model presentation

2.1. Classical equations

A continuous-wave FOPA, as showed in Fig. 1(a), is described by Maxwell's equations by assuming only a single mode, a real valued $\chi^{(3)}$-nonlinear fiber and only a single state of po-

larization [1]. In the following, we derive FOPA equations that include FWM, loss and Raman scattering for three monochromatic wave components, ω_1, ω_2, and ω_3. These waves always fulfil $\omega_1 < \omega_2 < \omega_3$ and $2\omega_2 = \omega_1 + \omega_3$, and they are all so close to the ZDF that FWM is efficient. The total electric field is written as

$$\mathbf{E}(\mathbf{r},t) = \frac{1}{2}\mathbf{x}\sum_{j=1,2,3} F_j(x,y)A_j(z)\exp(i\beta_j z - i\omega_j t) + \text{c.c.}, \tag{1}$$

where $F_j(x,y)$ is the transverse field distribution in the fiber, $A_j(z)$ is the slowly-varying complex field amplitude in units of $\sqrt{W}$, where W is Watts, and β_j is the wave number of mode j. By inserting Eq. (1) into the nonlinear wave equation [12], the following coupled amplitude equations may be derived:

$$\frac{\partial A_1}{\partial z} = i\gamma\left(\left[|A_1|^2 + 2(|A_2|^2 + |A_3|^2)\right]A_1 + A_2^2 A_3^* \exp(-i\Delta\beta z)\right), \tag{2}$$

$$\frac{\partial A_2}{\partial z} = i\gamma\left(\left[|A_2|^2 + 2(|A_1|^2 + |A_3|^2)\right]A_2 + 2A_1 A_3 A_2^* \exp(i\Delta\beta z)\right), \tag{3}$$

$$\frac{\partial A_3}{\partial z} = i\gamma\left(\left[|A_3|^2 + 2(|A_1|^2 + |A_2|^2)\right]A_3 + A_2^2 A_1^* \exp(-i\Delta\beta z)\right), \tag{4}$$

where γ is the nonlinear coefficient and $\Delta\beta = \beta_1 + \beta_3 - 2\beta_2$ is the wave number mismatch, which is calculated according to [1], and where it was assumed that all wave components have the same transverse field distribution. Due to energy conservation among the interacting waves, $\omega_2 - \omega_1 = \omega_3 - \omega_2$ is always fulfilled. Fiber loss is included by subtracting the term $\alpha/2\,A_j$ from the right hand side of each equation, where α is the loss coefficient.

Stimulated Raman scattering is usually described in equations of power, but due to the model of noise that we present here the equations must be in terms of the field amplitude. In Eq. (2) for wave ω_1, we add the effect of stimulated Raman scattering by the following consideration; since ω_1 is the smaller frequency, it receives Stokes scattering from both ω_2 and ω_3. These contributions are accounted for by the terms [13]

$$\frac{g_R^{21}}{2}|A_2|^2\left(n_T^{21} + 1\right)A_1 + \frac{g_R^{31}}{2}|A_3|^2\left(n_T^{31} + 1\right)A_1, \tag{5}$$

where $g_R^{ij} = 2\gamma f_R h_R(\Omega_{ij})$ is the Raman gain coefficient, $f_R = 0.18$ is the Raman fraction, h_R is the Raman response function (see below), $\Omega_{ij} = \omega_i - \omega_j$, and $n_T^{ij} = (\exp(\hbar|\Omega_{ij}|/k_B T) - 1)^{-1}$ is the phonon equilibrium number, where $\hbar$ is Planck's constant, k_B is Boltzmann's constant, and T is the temperature. The term $(n_T^{ij} + 1)$ implies that the Stokes process can take place even in the absence of any phonons, i.e. when $n_T^{ij} = 0$. Further, wave ω_1 also contributes to the waves ω_2 and ω_3 through the anti-Stokes process, which requires the presence of a phonon, and we account for that process in Eq. (2) with the terms

$$-\frac{g_R^{21}}{2}|A_2|^2 n_T^{21} A_1 - \frac{g_R^{31}}{2}|A_3|^2 n_T^{31} A_1. \tag{6}$$

In Eq. (3) for A_2, wave ω_2 relates to wave ω_3 equally to how wave ω_1 relates to wave ω_2 in Eq. (2). However, because wave ω_2 gives energy to wave ω_1 through the Stokes process, more energy must be taken from wave ω_2 than that which is given to wave ω_1. This is because the Stokes process implies the creation of a phonon that also contains energy. The resulting terms for the Stokes process in Eq. (3) become

$$-\frac{g_R^{21}}{2}|A_1|^2\left(n_T^{21} + 1\right)\frac{\omega_1}{\omega_2}A_2 + \frac{g_R^{32}}{2}|A_3|^2\left(n_T^{32} + 1\right)A_2, \tag{7}$$

where the factor ω_1/ω_2 accounts for the phonon energy. In the anti-Stokes process, in which wave ω_2 receives energy from wave ω_1, more energy must be added than that taken from wave ω_1 because the process involves the destruction of a phonon. Hence, the anti-Stokes terms in Eq. (3) become

$$\frac{g_R^{21}}{2}|A_1|^2 n_T^{21}\frac{\omega_1}{\omega_2}A_2 - \frac{g_R^{32}}{2}|A_3|^2 n_T^{32}A_2. \tag{8}$$

In Eq. (4), wave ω_3 relates to waves ω_1 and ω_2 equally to how wave ω_2 relates to wave ω_1 in Eq. (3). In total, the FOPA equations including loss and stimulated Raman scattering become

$$\begin{aligned}
\frac{\partial A_1}{\partial z} &= i\gamma\left(\left[|A_1|^2 + 2(|A_2|^2 + |A_3|^2)\right]A_1 + A_2^2 A_3^* \exp(-i\Delta\beta z)\right) \\
&\quad -\frac{\alpha}{2}A_1 + \frac{g_R^{21}}{2}|A_2|^2 A_1 + \frac{g_R^{31}}{2}|A_3|^2 A_1, \tag{9}
\end{aligned}$$

$$\begin{aligned}
\frac{\partial A_2}{\partial z} &= i\gamma\left(\left[|A_2|^2 + 2(|A_1|^2 + |A_3|^2)\right]A_2 + 2A_1 A_3 A_2^* \exp(i\Delta\beta z)\right) \\
&\quad -\frac{\alpha}{2}A_2 - \frac{g_R^{21}}{2}\frac{\omega_2}{\omega_1}|A_1|^2 A_2 + \frac{g_R^{32}}{2}|A_3|^2 A_2, \tag{10}
\end{aligned}$$

$$\begin{aligned}
\frac{\partial A_3}{\partial z} &= i\gamma\left(\left[|A_3|^2 + 2(|A_1|^2 + |A_2|^2)\right]A_3 + A_2^2 A_1^* \exp(-i\Delta\beta z)\right) \\
&\quad -\frac{\alpha}{2}A_3 - \frac{g_R^{31}}{2}\frac{\omega_3}{\omega_1}|A_1|^2 A_3 - \frac{g_R^{32}}{2}\frac{\omega_3}{\omega_2}|A_2|^2 A_3. \tag{11}
\end{aligned}$$

Note that the terms with n_T^{ij}, and hence the temperature dependence, have cancelled. We apply these equations to simulate FOPAs by setting $\omega_2 = \omega_p$, and if $\omega_s < \omega_p$, then $\omega_1 = \omega_s$ and $\omega_3 = \omega_i$, but if $\omega_s > \omega_p$, then $\omega_3 = \omega_s$ and $\omega_1 = \omega_i$.

The frequency-domain Raman response function is obtained by taking the imaginary part of the Fourier transform of the standard single-damped-oscillator model [14, 15],

$$h_R(t) = \exp(-t/\tau_2)\sin(t/\tau_1)\Theta(t), \tag{12}$$

where $\Theta(t)$ is a step function and $\tau_1 = 12.2$ fs and $\tau_2 = 32$ fs. It was shown in [16] that the real part of the Raman susceptibility has a significant impact on the phase-matching condition of FWM through induced refractive index changes; this was the case only for pump pulses with peak powers of 80 W and detuning frequency shifts of > 10 THz. Since we deal with CW sources of much lower power here, and detuning frequency shifts of < 6 THz, we assume that the refractive index changes caused by the real part of the Raman response function are negligible. We have included the nonlinear phase modulation and Raman interaction terms among all wave components, because Eqs. (9)–(11) are required to be valid when the pump depletes. We note that the model is valid in depletion in terms of interaction among the three wave components, while the generation of higher order FWM products [17] has been disregarded. This approximation becomes gradually less valid in the deep nonlinear gain regime.

Equations (9)–(11) describe the evolution of the complex field amplitude of each frequency component at any point in the amplifier; we calculate the gain of the signal as

$$G(z) = \frac{\langle |A_s(z)|^2 \rangle}{\langle |A_s(0)|^2 \rangle}, \tag{13}$$

where the mean value of the normalized field-amplitude squared is calculated based on field ensembles as outlined below; $|A_s|^2$ is proportional to the photon number of the signal. We assume

that an electric field of power P is related to its number of photons n by $P = n\hbar\omega B_0$, where B_0 is the frequency domain bandwidth. In terms of gain and evaluation of noise fluctuations, the constant factor $\hbar\omega B_0$ plays no role. In the case of PI amplification, the SNR of the signal for direct detection is defined as the square of the mean photon number divided by the photon number variance [8, 10, 18]

$$SNR_{PI} = \frac{\langle |A_s(z)|^2 \rangle^2}{\text{Var}(|A_s(z)|^2)}. \tag{14}$$

In the PS case, however, many have discovered that the definition Eq. (14) leads to a 3-dB improvement of the SNR of both signal and idler simultaneously [4, 8, 19] as opposed to the 0-dB change in SNR predicted originally [3]. Therefore, a definition based on all input and output information is used in this work [11],

$$SNR_{PS} = \frac{\langle |A_s(z)|^2 + |A_i(z)|^2 \rangle^2}{\text{Var}(|A_s(z)|^2 + |A_i(z)|^2)}. \tag{15}$$

The NF of the amplifier is SNR_i/SNR_o for both the PI and PS cases, in which i and o denote *input* and *output*, respectively. It is noted that the 3-dB improvement of the SNR in a PSA is a real effect that has been measured based on a copier-loss-amplifier scheme [4], in which the copier is a PI parametric amplifier that generates an idler with a corresponding 3-dB penalty in the signal SNR.

2.2. Simulation of the coherent state

For accurate simulations of quantum noise during parametric amplification, the classical input fields should resemble the quantum coherent state and, thus, be defined in accordance with quantum mechanics. One approach to achieve this is to add a small fluctuation term to the mean amplitude of each input field, $A_j = \bar{A}_j + \delta A_j$. The fluctuations must have the properties $\langle \delta A_j \rangle = 0$, $\langle \delta A^2 \rangle = 0$ and $\langle |\delta A|^2 \rangle = 1/2$ to ensure that the total field, A_j, holds one half photon on average in the absence of any mean field, $\bar{A}_j$.

Another approach is to add normally distributed fluctuations to the real and imaginary parts of the input fields, thus simulating the fluctuations in the two quadratures of the quantum electric field. The variances of these fluctuations are obtained directly from the commutator relation of the quadrature operators, $\hat{x}$ and $\hat{p}$, i.e. $[\hat{x}, \hat{p}] = i/2$, which dictates that $\text{Var}(\hat{x})\text{Var}(\hat{p}) \geq 1/16$, so in a non-squeezed state of light we have $\text{Var}(\hat{x}) = \text{Var}(\hat{p}) = 1/4$ in units of photons [20]. In this work, we use the second approach and thus define the input fields as

$$A_j = \bar{x}_j + \delta x_j + i(\bar{p}_j + \delta p_j), \tag{16}$$

where $\bar{x}_j$ and $\bar{p}_j$ are related to the classical amplitude and phase by $\bar{x}_j = A_j \cos(\phi_j)$ and $\bar{p}_j = A_j \sin(\phi_j)$, and the fluctuations have the properties $\langle \delta x_j \rangle = \langle \delta p_j \rangle = 0$ and $\text{Var}(\delta x_j) = \text{Var}(\delta p_j) = 1/4$, where $j \in \{p, s, i\}$ and δx_j and δp_j are uncorrelated. The indeterministic nature of the quantum electric field is captured classically by using Eq. (16) to create an ensemble of classical fields from which we calculate the photon mean value and variance,

$$\langle n_j \rangle = \langle |A_j|^2 \rangle = \bar{x}_j^2 + \bar{p}_j^2 + 1/2, \tag{17}$$

$$\text{Var}(n_j) = \langle |A_j|^4 \rangle - \langle |A_j|^2 \rangle^2 = \bar{x}_j^2 + \bar{p}_j^2 + 1/4. \tag{18}$$

The electric field is here normalized to represent the photon number instead of power. Evidently, Eq. (17) shows that by adding the fluctuations δx_j and δp_j we explicitly include the energy of the vacuum fluctuations in the model, identified by the term of 1/2 photon in average. By comparing Eqs. (17) and (18), we also confirm that for large photon numbers $SNR_j = \bar{x}_j^2 + \bar{p}_j^2$, which is proportional to the photon number, as one would expect for a coherent state.

2.3. Spontaneously emitted photons in the fiber

During propagation in the amplifier, spontaneously generated photons distort the signal quality. Here, we focus on two unavoidable sources of noise in a fiber; loss induced noise (LIN) and spontaneous Raman scattering (SRS). Both effects are included by adding fluctuation terms to all propagating fields at a finite number of positions in the fiber amplifier, e.g. in every step along the fiber of the numerical differential-equation solver.

LIN originates from the coupling of the electric field to a scattered (loss) mode, which contains vacuum fluctuations, and the effect of which can be modelled as a two-port beam splitter [21]. For our purpose, however, it is simpler to consider the variance of each quadrature, which cannot decrease below 1/4 due to loss alone. In the semi-classical model large loss implies that all fields decay asymptotically to zero, hence also the quadrature variances, so to obey the uncertainty principle we add a fluctuation term in each numerical step to both the real and imaginary parts of all propagating fields. The statistical properties of the fluctuation term are

$$\langle \delta a_{LIN} \rangle = 0, \tag{19}$$
$$\mathrm{Var}(\delta a_{LIN}) = \alpha \Delta z/4, \tag{20}$$

where Δz is the step size and α is the loss coefficient of Eqs. (9)–(11). This value of the fluctuation variance ensures that the quadrature variances decay to 1/4 in the limit of large losses. We also note that a passive device (e.g. a fiber with attenuation) is well-known to influence a transmitted signal with a signal-to-noise degradation equal to the loss. We verified that the model of LIN presented here captures this result correctly.

SRS originates from the coupling of the electric field to thermal phonon states in the medium of propagation and consists of two distinct contributions: 1) the spontaneous annihilation of a high-frequency photon in the creation of an optical phonon and a lower-frequency photon, both with random phases (Stokes process), and 2) the spontaneous annihilation of a low-frequency photon and an optical phonon in the creation of a higher-frequency photon with random phase (anti-Stokes process). The two processes happen with unequal probability, because the anti-Stokes process requires the presence of a phonon, while the Stokes process does not. Referring back to Eqs. (9)–(11), wave ω_3 scatters spontaneously to waves ω_1 and ω_2 in the Stokes process, and wave ω_1 scatters spontaneously to waves ω_2 and ω_3 in the anti-Stokes process. Wave ω_2 scatters spontaneously to wave ω_1 in the Stokes process and to wave ω_3 in the anti-Stokes process. Spontaneous Stokes (S) scattering is accounted for by adding fluctuation terms to the real and imaginary parts of each field with the properties

$$\langle \delta a_S \rangle = 0, \tag{21}$$
$$\mathrm{Var}(\delta a_S) = (1 + n_T(\Omega_{jk}))g_R(\Omega_{jk})|A_j|^2 \Delta z/2, \tag{22}$$

where k denotes the field that receives scattering and j denote the field that gives scattering. Spontaneous anti-Stokes (AS) scattering is accounted for in a similar way with a fluctuation term with the properties

$$\langle \delta a_{AS} \rangle = 0, \tag{23}$$
$$\mathrm{Var}(\delta a_{AS}) = n_T(\Omega_{jk})g_R(\Omega_{jk})|A_j|^2 \Delta z/2. \tag{24}$$

Note that SRS is temperature depended, and that spontaneous Stokes scattering can take place in the absence of phonons, but spontaneous anti-Stokes scattering cannot. The variance of δa_S and δa_{AS} was chosen so that the consequent change in signal power is in accordance with the classical power equations of the Raman amplifier [22].

3. Amplifier noise in the linear gain regime

In this section, we analyze the noise properties of a FOPA configured as shown in Fig. 1(a), in the linear gain regime, to show that 1) the presented semi-classical model agrees with known quantum-based results and 2) the effects of LIN and SRS. For a PIA the parametric gain and NF can be calculated in the linear gain regime assuming that loss and Raman scattering may be disregarded to be [1, 8, 10]

$$G_{PI}(z) = 1 + \left[\frac{\gamma P_p}{g} \sinh(gz) \right]^2, \tag{25}$$

$$NF_{PI}(z) = 1 + \frac{G_{PI}(z) - 1}{G_{PI(z)}}, \tag{26}$$

where $g^2 = -\Delta\beta(\Delta\beta/4 + \gamma P_p)$ is the parametric gain coefficient and P_p is the constant pump power. Similar but more complicated expressions for the PS parametric gain and NF are derived in [18] for the linear gain regime; in general the PS amplification process depend also on the input idler phase and amplitude, whereas the PI process does not. However, if we assume ideal phase matching, $\Delta\beta = -2\gamma P_p$ (which determines the signal wavelength relative to the pump wavelength for a specific fiber), and choose the relative phase of the pump, signal and idler to be $\theta_{rel} = 2\phi_p - \phi_s - \phi_i = -\pi/2$, the signal and idler grow according to

$$P_s(z) = \left(\sqrt{G_{PI}(z)P_{s,0}} + \sqrt{(G_{PI}(z) - 1)P_{i,0}} \right)^2, \tag{27}$$

$$P_i(z) = \left(\sqrt{G_{PI}(z)P_{i,0}} + \sqrt{(G_{PI}(z) - 1)P_{s,0}} \right)^2, \tag{28}$$

where $P_{s,0}$ and $P_{i,0}$ are the signal and idler input powers, respectively. The PS parametric gain is then $G_{PS}(z) = P_s(z)/P_{s,0}$. Under the same conditions, the PS NF reduces to

$$NF_{PS}(z) = (P_{s,0} + P_{i,0}) \cdot \frac{\left(\sqrt{G_{PI}P_s} + \sqrt{(G_{PI} - 1)P_i} \right)^2 + \left(\sqrt{G_{PI}P_i} + \sqrt{(G_{PI} - 1)P_s} \right)^2}{(P_s + P_i)^2}. \tag{29}$$

Note that in the case of equal signal and idler input powers, the PS NF reduces to 1 (0 dB) independent of the gain.

Figure 2(a) shows simulations of the parametric gain and NF for both a PIA (gray) and PSA (black) versus fiber position z with and without loss and Raman contributions; the ensemble size is 5×10^4. In the PSA case, equal signal and idler input powers were chosen. The numerical results without loss and Raman scattering compare excellently to the analytical expressions (the gain curves with loss and Raman scattering are omitted for visual reasons), which means that the field ensemble behaves as a classical parametric amplifier on average. The effect of including loss and Raman scattering on the parametric gain is minor, but the NF increases significantly in both the PI and PS cases, thus destroying the 3-dB and 0-dB NFs, respectively, as predicted by quantum theory; this result is in agreement with other theoretical studies of Raman scattering in parametric amplifiers [10, 11] and with experiments [18, 23]. It was verified in subsequent simulations that the noise contribution from LIN is insignificant compared to that from SRS.

Figure 2(b) shows gain and NF spectra around the pump wavelength, λ_p, where the analytic expressions are now omitted; from the gain curves in the top plot the high-gain regions stand out clearly. The NF curves in the bottom plot show the 3-dB NF floor of the PIA (gray) without loss and Raman scattering, and an asymmetric increase in the NF all over the spectrum where loss and Raman scattering are included. The distortion of the signal in the latter case is due
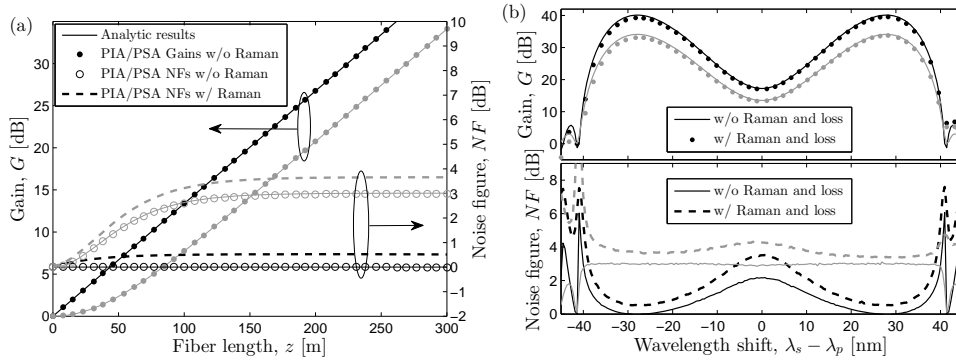
Fig. 2. (a) PIA (gray) and PSA (black) gains and NFs versus fiber length with and without the Raman effect and loss (the gain with Raman and loss are not shown; line styles apply to both PIA and PSA curves), (b) Gain and NF spetrca at the amplifier output ($z = 300$ m), which show the effect of SRS and LIN on the NF. Parameters: $P_{p,0} = 1.4$ W, $P_{s,0} = 10^{-7}$ W, $\lambda_p = 1560.7$ nm, $\lambda_0 = 1559$ nm, $\gamma = 11$ $(\mathrm{W\,km})^{-1}$, $\partial D/\partial \lambda = 0.03$ ps/(nm^2 km), $\alpha = 0.4$ dB/km, $T = 300$ K, and $\Delta z = 1$ m.

to the random phase of the spontaneously emitted photons of LIN and SRS, which increase the variance in the number of photons without increasing the mean number. In the numerical model, the signal is represented by an ensemble that forms a circular shape in phase space, and the addition of δa_{LIN} and δa_{SRS} in each step increases the radius of the circle without moving its center. The local increase of the NF around the pump wavelength is caused by the rapid increase in the phonon equilibrium number for vanishing wavelength shifts.

In contrast to the PI NF, which is almost independent of the signal wavelength, the PSA NF is seen to be 0 dB only at the ideal phase matching condition for maximum gain, which was defined above. However, through the entire spectrum of high gain, the PSA NF curve without loss and Raman scattering breaks the 3-dB quantum limit of the PI process, and we further observe that this holds true in the high-gain regions even when loss and Raman scattering are taken into account. We conclude that this result confirms the potential of the PSA as a low-noise component in future all-optical networks.

4. Amplifier noise in the nonlinear gain regime

In the linear gain regime, we observe that our simulations agree with known quantum results; therefore, we apply the model to the gain saturated regime, where it is difficult to describe the quantum noise properties of parametric processes quantum mechanically. We focus separately on the signal and the pump noise properties, respectively, and we limit our investigation to the case of a PIA.

4.1. Quantum noise on gain-saturated signal

To simulate the complete depletion of the pump, we increase the input signal power to $P_{s,0} = 10^{-4}$ W and keep all other parameters unchanged. The phase-matching condition for maximum gain, $\Delta \beta = -2\gamma P_p$, has two solutions in terms of signal wavelength (as seen in the top plot of Fig. 2(b)); in the linear gain regime the two solutions give identical gain in the absence of Raman scattering and slightly different gains with Raman scattering included. In the gain-saturated regime, however, where not only the pump scatters energy to higher wavelengths but also the lower-wavelength sideband does, the gain spectrum becomes highly asymmetrical, and
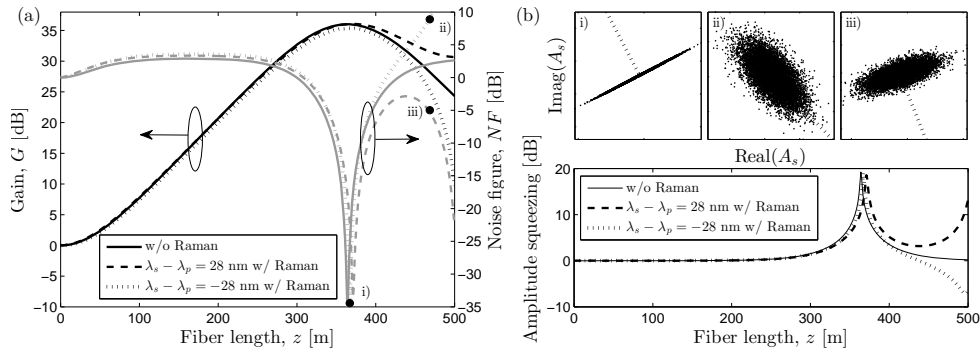
Fig. 3. (a) Signal gain (black) and NF (gray) of a depleted PIA without loss and Raman scattering (solid lines), and with loss and Raman scattering (dashed lines). (b) The top plots show constellation diagrams of the signal at the positions i)-iii) in (a), where loss and Raman scattering are included in all of them; the scalings in the three diagrams are not equal, so the sizes of the ensembles cannot be compared, only their shapes (the dotted lines point towards the origins of the phase-space diagrams). The bottom plot shows the degree of amplitude squeezing through the amplifiers with and without loss and Raman scattering. All plots indicate that neglecting Raman scattering beyond full pump depletion leads to a significant error. The parameters are the same as in Fig. 2, but with $P_{s,0} = 10^{-4}$ W.

we therefore include both solutions in our analysis.

Figure 3(a) shows the gain (black) and NF (gray) for a PIA with and without loss and Raman scattering. We observe that as the gain starts to saturate the NF decreases, and at full pump depletion the NF reaches -35 dB without loss and Raman scattering, and -32 dB with loss and Raman scattering, respectively. The explanation for the drastic increase in the SNR is found in the top plots of Fig. 3(b), where constellation diagrams of the signal are shown (the dotted lines point toward the origins of the phase-space diagrams). In the linear gain regime, the signal has a circular shape due to the uncorrelated noise in the two quadratures of the electric field. At position i) the field ensemble (including loss and Raman scattering) has been squeezed in amplitude thus reducing the photon number variance while maintaining the mean photon number. Evidently, such behaviour increases the photon number-based SNR. Notice that as the signal enters the depletion regime after being amplified, its fluctuations are much larger than those of vacuum. Therefore, the squeezed states shown in diagrams i)-iii) do not show quantum squeezing in which the fluctuations of one quadrature are smaller than the vacuum fluctuations, at the cost of larger fluctuations in the other quadrature. The concept of amplitude regeneration of optical signals in gain-saturated parametric amplifiers has been demonstrated several times [24–27].

Beyond full pump depletion the signal power decreases and the NF increases again, but as argued above the gain depends on which side band of the pump is considered. The NF is affected similarly, but not only from the difference in gain; constellation diagrams ii) and iii) show that the higher wavelength signal ensemble is squeezed in amplitude, whereas the lower wavelength signal ensemble is broadened in amplitude. The latter leads to the increasing NF shown in Fig. 3(a) as the dotted line.

The bottom plot of Fig. 3(b) gives a complete overview of the degree of amplitude squeezing in the two cases with loss and Raman scattering, and the one without loss and Raman scattering. The degree of amplitude squeezing is defined as $\sigma_{q_2}/\sigma_{q_1}$, where σ_{q_1,q_2} are the standard deviations on two axes defined in a local coordinate system with origins at the center of the
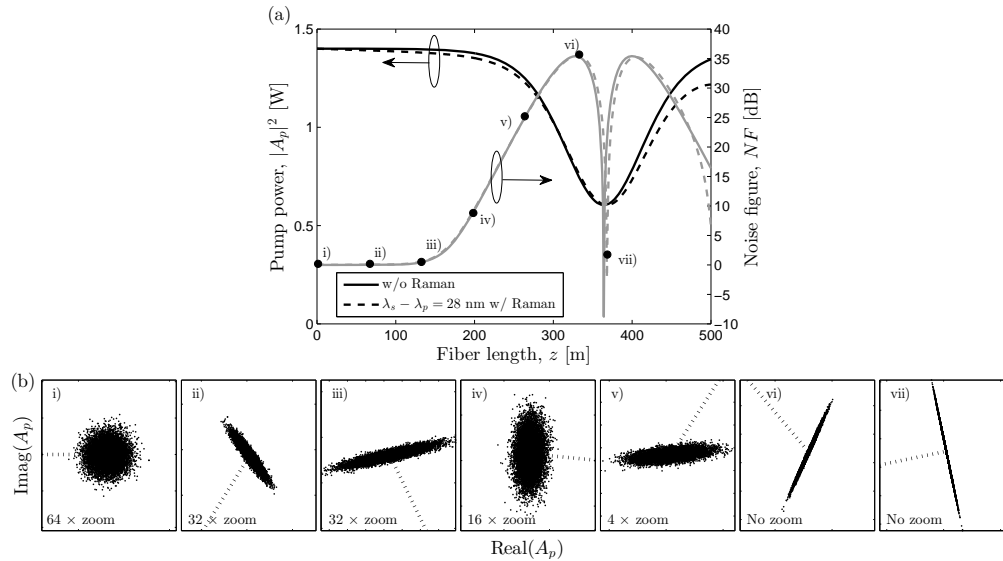
Fig. 4. (a) Pump power and NF through a PIA with and without loss and Raman scattering. The dots i)-vii) denote the positions to which the constellation diagrams in (b) belong, where i) $z = 0$ m, ii) $z = 67$ m, iii) $z = 133$ m, iv) $z = 200$ m, v) $z = 269$ m, vi) $z = 332$ m and vii) $z = 369$ m; loss and Raman scattering are included in all of them. The scaling on the axes of all the diagrams are equal except for the denoted zooms, so the sizes and shapes of the ensembles can be compared; the diagrams show the case with loss and Raman scattering. The parameters are the same as in Fig. 3.

ensemble. The axis q_1 is parallel to the radial direction (amplitude) and q_2 is parallel to the tangential direction (phase) of the phase-spaces shown in the diagrams i)-iii). From the results of Fig. 3 we further conclude that until full depletion of the pump is achieved, Raman scattering plays only a minor role in the dynamics of the FOPA; after the point of full depletion, however, a significant error occurs if Raman scattering is neglected.

4.2. Quantum noise on depleted pump

Because the pump is usually treated as a classical constant, its quantum noise dynamics have never been given much attention. Figure 4 shows the quantum noise properties of the pump from the same simulation that generated the results of the signal in Fig. 3. Plot (a) shows the pump power (black) and, as expected, it is constant in the linear gain regime ($z = 0$ m to $z \approx 180$ m). Thereafter, it gives approximately half its power to the signal and idler (full depletion is not achieved at the phase-mismatch of the chosen signal wavelength) and receives it back again. Stimulated Raman scattering causes the backward transfer to be incomplete. The NF (gray) is observed to be more complex than the NF of the signal: the curve increases to > 35 dB with decreasing power until the largest possible depletion, where the NF drops to < -5 without loss and Raman scattering dB and < 5 dB with loss and Raman scattering, respectively. In contrast to the signal NF, Raman scattering has only a minor influence on the pump NF.

Figure 4(b) shows constellation diagrams of the pump ensemble at the selected points i)–vii) in (a) including loss and Raman scattering, and they show a complex development with two properties that are not detectable in the NF curve: 1) even though the amplitude variance of the pump remains approximately constant in i)–iii) (constant NF curve) more phase noise is introduced. This is clearly seen in diagrams ii) and iii), where the ensembles have ellipsoidal

shapes compared to the circular shape in diagram i). As depletion is approached, the ensemble grows in all directions (the scales on the axes of all diagrams are equal except for the denoted zooms) as seen in iv)–vii), though the phase variance grows faster than the amplitude variance making the ensemble more ellipsoidal. 2) the broadening of the ensemble in phase is not orthogonal to the radial direction in phase space. Furthermore, the angle of broadening changes through ii)–vi) and the broadening is noticed to be orthogonal in iv) and vii). Comparing vi) and vii), evidently the ensemble is squeezed in amplitude as full pump depletion is reached. This squeezing is, as it was for the signal, the cause of the drop in the NF curve in plot (a); in diagram vi) the degree of amplitude squeezing is 22.0 dB as defined by above.

From the results of Fig. 4 we conclude that the pump takes an active part in the process of parametric amplification in a fiber, and the noise properties presented here are not special features of Raman scattering, but inherent effects of FWM. Clearly, a parameter as simple as the SNR Eq. (14) is not sufficient to describe the dynamics of the pump fluctuations. However, a thorough investigation of the pump–signal quantum noise interactions is outwith the scope of this paper.

5. Conclusion

In this paper, we have presented a semi-classical method for describing quantum noise in parametric processes. We have chosen to focus on the simplest scheme for parametric amplification in a fiber, modulation interaction (see Fig. 1), and presented the governing equations including loss, and stimulated and spontaneous Raman scattering.

In the linear gain regime of the amplification process, we found that the semi-classical method had excellent agreement with fully-quantum approaches when loss and Raman scattering were omitted. When both effects were included, we observed an increase in the NF of both PIAs and PSAs, thus destroying the predicted quantum-limited 3-dB and 0-dB NFs, respectively. Loss and Raman scattering are unavoidable in silica fibers, but contrary to vacuum fluctuations they depend on experimental parameters, so the set-up can be tailored to minimize their impacts.

The nonlinear gain regime, in which the noise properties of parametric processes are not yet described by quantum mechanics, is also accessible in the semi-classical method. Here, we show that as the signal depletes the pump, FWM causes the generation of an amplitude-squeezed state of light. Because the SNR is based on only the photon-number mean and variance, the squeezing induces a NF of < -30 dB. Loss and Raman scattering only influence this result to a minor degree; beyond the point of full depletion, however, we find that disregarding loss and Raman scattering leads to a significant error.

One more distinct feature of the semi-classical approach is the possibility of investigating the quantum noise on the pump of the amplifier. In such an investigation, we conclude that the fluctuations of the pump are affected significantly by FWM with the signal and idler, and that the SNR is too simple a concept to describe the quantum noise dynamics even in the linear gain regime. Loss and Raman scattering do not affect significantly the conclusions drawn from investigations of the pump.

Acknowledgment